Two long-axis dimensions of hippocampal cortical integration support memory function across the adult lifespan

Kristin Nordin[1,2,3], Robin Pedersen[3,4,5], Farshad Falahati[1,2], Jarkko Johansson[4,6], Filip Grill[7], Micael Andersson[4,5], Saana M. Korkki[1,2], Lars Bäckman[1,2], Andrew Zalesky[8,9], Anna Rieckmann[4,6,10], Lars Nyberg[4,5], Alireza Salami[1,2,3,4,5]

[1]Department of Neurobiology, Care Sciences, and Society, Karolinska Institutet, Solna, Sweden
[2]Aging Research Center, Karolinska Institutet and Stockholm University, Solna, Sweden
[3]Wallenberg Centre for Molecular Medicine, Umeå University, Umeå, Sweden
[4]Umeå Center for Functional Brain Imaging, Umeå University, Umeå, Sweden
[5]Department of Integrative Medical Biology, Umeå University, Umeå, Sweden
[6]Department of Radiation Sciences, Umeå University, Umeå, Sweden
[7]Donders Centre for Cognitive Neuroimaging, Radboud University, Nijmegen, the Netherlands
[8]Department of Biomedical Engineering, the University of Melbourne, Melbourne, VIC, Australia
[9]Department of Psychiatry, the University of Melbourne, Melbourne, VIC, Australia
[10]Department of Psychology, University of the Bundeswehr Munich, Germany

Ethics approval: This study was approved by the Regional Ethical board and the local Radiation Safety Committee in Umeå, Sweden.

Conflict of interest statement: The authors declare no conflict of interest.

Corresponding author: Kristin Nordin
Karolinska Institutet
Aging Research Center
Tomtebodavägen 18A
171 65 Solna, Sweden
E-mail: kristin.nordin@ki.se

Abstract

Multiple overlapping spatial modes define the organization of hippocampal function along its longitudinal and transverse axes, but remain unexplored in relation to behavior and to cognitive decline in aging. Here, we identify two long-axis modes of hippocampal-cortical functional connectivity (FC), each representing a distinct neurocognitive cortical hierarchy: a principal anterior-posterior gradient reflecting a task-positive/task-negative cortical motif, and a second-order gradient separating the middle hippocampus from anterior and posterior ends, reflecting unimodal-transmodal cortical organization. The second-order gradient predicted episodic memory and mirrored hippocampal dopamine D1 receptor distribution, capturing shared functional and neuromolecular organization. Older age was associated with less gradual FC change along gradients, and a youth-like gradient profile was linked to preserved memory – highlighting age-related gradient dedifferentiation as a marker of cognitive decline. Our results indicate that hippocampal function stands to inform general principles of brain organization, and emphasize a critical role of long-axis organization in memory across the lifespan.

Key words: Aging, Anteroposterior axis, Connectopic mapping, Dopamine, Episodic memory, Gradient mapping

The hippocampus plays a critical role in human behavior beyond its well-established involvement in memory and spatial navigation[1–5]. Contemporary views hold that its broad involvement in cognition emerges through the combination of its intrinsic circuitry and its widespread cortical connections – placing it at the interface of multiple behavioral systems[3,6,7]. Characterizing organizational principles of hippocampal integration with the larger cortical landscape is therefore key to our understanding of its contribution to cognition and to the many diseases associated with its dysfunction[8–13].

Animal models[14,15], together with histological and functional descriptions in humans[16–20], emphasize the hippocampus transverse (mediolateral) and longitudinal (anteroposterior) axes in determining its functional organization, contribution to behavior[21–23], and vulnerability to neurological disease[24,25]. In humans, functional analogues of the hippocampus canonical internal circuitry and its anatomical connections with cortical areas have successfully been provided by resting-state functional magnetic resonance imaging (fMRI)[18,19,26,27], at a coarse scale confirming the anteroposterior gradient in connectivity observed in the animal literature[14,28–30]. Moreover, spatial variation in functional cortical connectivity along the hippocampus longitudinal axis has been reported as informed by structural covariance[20], gene expression[31], and transitions in anatomical connections[32,33]. Despite the consistency by which this anteroposterior organizational dimension emerges[34], significant questions remain regarding the spatial distribution of long-axis connectivity patterns across cortex and their contribution to behavior.

Lack of consensus is especially evident in terms of the hippocampus functional connectivity with the default-mode network (DMN[35]), encompassing core areas of the brain's system for memory-guided behavior[7,36–38]. Several studies primarily attribute integration with the DMN to the posterior hippocampus[7,18,27,39–41], consistent with its anatomical connections to midline posterior parietal areas[28,42]. Other sources emphasize the anterior hippocampus as

driving connectivity with the DMN[31,43–45], on the basis of its anatomical connections with ventromedial prefrontal areas[28]. These inconsistencies ultimately limit our understanding of hippocampal functional specialization, and the impact on cognition of the heterogeneous vulnerability to aging and disease observed along the hippocampus longitudinal axis[25,46]. We propose that inconsistencies in part stem from overlooking multiple overlapping and complementary modes of hippocampal function, not discernable through traditional parcellation-based approaches, which assume homogeneous function within distinct, pre-defined, portions of the hippocampus.

Driven by advances in neuroimaging data analysis, macroscale organization of neocortical function is increasingly understood in terms of overlapping topographic modes (i.e., gradients of functional connectivity) reflecting differentiation across distinct neurofunctional hierarchies[47–49]. Consistently described in the literature as the principal organizational axis of cortical function is a unimodal-transmodal gradient, at one end anchored in DMN-areas of association cortices, and at the other, in unimodal sensory and motor cortices[47–49]. Higher-order cortical gradients describe functional differentiation between poles of visual and somatomotor areas, as well as between neural communities at one end involved in the formation of representations from sensory input (e.g., visual, somatosensory, and DMN areas) and at the other, those involved in the modulation of these representations (e.g., frontoparietal areas of attention and control)[48,50]. The hippocampus has recently been proposed to harbor local representations of these macroscale cortical gradients, conveyed by gradual change in cortical connectivity along multiple overlapping spatial modes[50–52].

Whereas gradient-based observations align with traditional studies in describing a principal anteroposterior mode of variation in cortical connectivity, they additionally characterize orthogonal long-axis and transverse variation[50,51,53]. This may suggest that the linear, anteroposterior, perspective currently dominating the literature only constitutes a partial

representation of hippocampal long-axis functional organization. Critically, there is limited insight into how these distinct organizational gradients contribute to human behavior. No study to date has concomitantly mapped these gradients of cortico-hippocampal connectivity onto inter-individual differences in behavior. This is of particular importance given the recent debate on which specific aspects of brain organization underlie gradients of functional connectivity[54,55]. Critically, current gradient-based findings remain restricted to young adults, and, to overlapping samples of young participants (i.e. the Human Connectome Project[56]). In the present study, we address these caveats by characterizing the multidimensional organization of hippocampal-cortical connectivity across the adult human lifespan and mapping individual differences in topographic properties of gradients onto behavioral and molecular phenotypes.

Dopamine (DA) is one of the most important modulators of hippocampus-dependent function[57,58], and is considered to influence the brain's functional architecture through synaptic modulation enhancing specificity of neuronal signaling[59,60]. Animal models suggest heterogeneous DA innervation patterns[61–64], and spatial variation in postsynaptic DA receptors[65], across both transverse and longitudinal hippocampal axes, likely allowing for separation between DA modulation of distinct hippocampus-dependent behaviors[57]. Moreover, the human hippocampus has been linked to distinct DA circuits on the basis of long-axis variation in functional connectivity with midbrain and striatal regions[66–68]. We therefore tested the hypothesis that the organization of hippocampal cortical connectivity partly reflects the underlying distribution of hippocampal DA receptors. Based on recent findings revealing a unimodal-transmodal organization of the most abundantly expressed DA receptor subtype, D1 (D1DR), across cortex[69], consistent with observations in non-human primates[70], we predicted predominant spatial correspondence for any hippocampal gradient conveying a unimodal-transmodal pattern across cortex.

Finally, in cognitively healthy older adults, functional isolation of anterior and posterior hippocampal regions from prefrontal areas and large-scale cortical networks has been described in association with their dysfunction during memory encoding and retrieval[71–73]. Recent studies suggest that this disconnection could be driven by the spatial patterns in which Alzheimer's pathology accumulates[74–76]. Comprehensively investigating overlapping modes of cortico-hippocampal interactions as determined by the hippocampus anteroposterior axis may as such be of particular importance to identifying early markers of cognitive decline in older age and preclinical dementia.

Here, we report three hippocampal gradients of functional connectivity displaying distinct correspondence to a) canonical gradients of cortical functional organization, b) the organization of hippocampal DA receptors, and c) individual differences in hippocampus-dependent memory function. Age-sensitivity of gradients was assessed across the adult lifespan, and data-driven classification identified older adults exhibiting a youth-like gradient profile and superior memory function as distinct from age-matched older counterparts, indicating a functional significance of preserved hippocampal topography in older age.

Results

Multiple dimensions of hippocampal cortical integration across the adult lifespan

Connectopic mapping[77] was applied to resting-state fMRI data (n=180, 90 men/90 women; 20-79 years; mean age = 49.8±17.4) from the DyNAMiC study[78]. For replication, we used an independent sample of 224 adults (122 men/102 women; 29-85 years mean age = 65.0±13.0) from the Betula project[79,80]. Connectopic mapping was used to extract the dominant modes of functional connectivity within the hippocampus based on non-linear manifold learning (Laplacian eigenmaps) applied to a similarity matrix derived from functional connectivity fingerprints computed between each hippocampal voxel and each voxel within neocortex. This identified a set of orthogonal connectopic maps (i.e. eigenvectors) describing overlapping

connectivity topographies (i.e. gradients) within the hippocampus. Gradients were computed at subject level, and at group level across the sample, separately for the left and right hippocampus. We analyzed the first three gradients, together explaining 63% and 71% of the variance in left- and right-hemispheres, respectively. Furthermore, this number corresponded to a clear elbow in the scree plot (Supplementary Figure 1).

The principal gradient (G1), explaining 44% and 53% of the variance in left and right hemispheres, was organized along the hippocampus longitudinal axis, conveying gradual anterior-to-posterior variation in hippocampal-cortical connectivity (Figure 1A). This pattern of connectivity change is illustrated by dividing subject-level G1 connectopic maps into 23 long-axis bins of ~2mm and plotting the average gradient values as a function of their distance from the most anterior hippocampal voxel[53] (Figure 1B). The second-order gradient (G2), explaining 11% of the variance in both hemispheres, expressed a secondary long-axis gradient organized from the middle hippocampus towards anterior and posterior ends (Figure 1A-B). Finally, the third-order gradient (G3: explaining 8% and 7% of the variance), reflected variation along the hippocampus transverse axis, such that inferior-lateral parts of the hippocampus were separated from medial-superior parts (Figure 1A). This pattern was most pronounced in the anterior hippocampus. Inspecting G3 across sample-specific segmentations of cornu ammonis (CA1-3), dentate gyrus (DG/CA4), and subiculum subfields suggested that while CA1-3 reflected the full extent of the gradient, and DG/CA4 variation around its center, the subiculum reflected only the most inferior section of the gradient (Supplementary Figure 2). The three gradients were highly reproducible in the independent replication data set (Supplementary Figure 3). Correspondence between samples was determined by spatial correlations between gradient pairs (left hemisphere: G1: $r = 0.990$, $p < 0.001$; G2: $r = 0.946$, $p < 0.001$; G3: $r = 0.918$, $p < 0.001$; right hemisphere: G1: $r = 0.996$, $p < 0.001$; G2: $r = 0.969$, $p < 0.001$; G3: $r = 0.897$, $p < 0.001$).

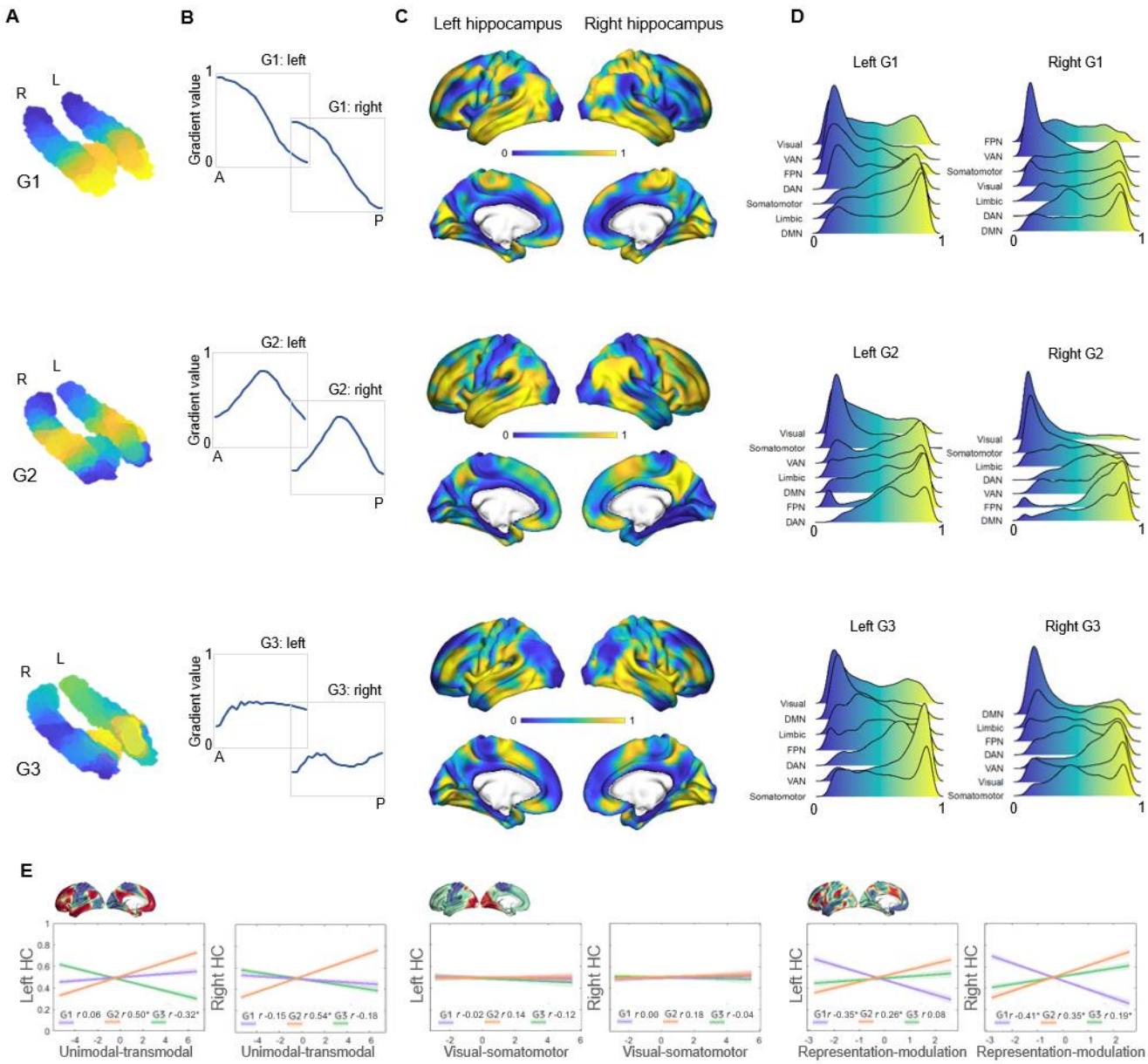

Figure 1. Topographic gradients of hippocampal cortical connectivity. A) The first three hippocampal connectopic maps (G1-G3), explaining 67% of the variance across left and right hemispheres. Similar colors convey similar patterns of cortical connectivity. Values range between 0 (blue) and 1 (yellow). B) Plots convey change in connectivity along the anteroposterior hippocampal axis. Mean values from 23 hippocampal bins (each ~2mm) are plotted against their distance (in mm) from the most anterior hippocampal voxel. Values were estimated based on subject-level gradients and averaged across participants. G1 conveys gradual change in connectivity along an anteroposterior gradient. G2 conveys gradual change in connectivity along a second-order long-axis gradient, separating the middle hippocampus from anterior and posterior ends. G3 conveys close to no change in connectivity along the longitudinal axis, with connectivity change instead organized in a primarily medial-lateral gradient. C) Cortical projections for G1, G2, and G3. Values range between 0 (blue) and 1 (yellow). D) The order of cortical networks in gradient space. Density plots visualize the distribution of gradient values for each of the seven networks in the Yeo 2011 parcellation (Yeo et al., 2011). E) Correlations between the cortical patterns of hippocampal gradients and the three primary gradients of cortical functional organization which are exemplified at the top of each graph (Margulies et al., 2016).

Hippocampal gradients reflect distinct dimensions of macroscale cortical organization

The projection of G1 onto cortex conveyed a pattern linking medial orbitofrontal, temporolimbic, and medial parietal regions at the anterior end of the gradient with occipital and frontoparietal regions at the posterior end (Figure 1C). To characterize the cortical organization of G1, we computed gradient values within seven cortical networks[81], and examined their position in gradient space. Network-specific density curves placed the DMN, limbic, and somatomotor networks at anterior-to-middle parts of the gradient, whereas visual, ventral attention, and frontoparietal networks toward the posterior end of the gradient (Figure 1D). In contrast, G2 exhibited a unimodal-transmodal pattern across cortex, linking the middle hippocampus to frontal and posterior parietal regions, and anterior and posterior hippocampal ends to somatomotor and occipital regions (Figure 1C). Consistently, networks mapped onto G2 placing the DMN and frontoparietal networks at one end, and visual and somatomotor networks at the other (Figure 1D). Across cortex, G3 primarily separated temporal and insular areas from medial parietal and medial frontal areas (Figure 1C). Aligning with cortical connectivity previously reported for hippocampal subfields[27,51,82], areas of the DMN most strongly mapped onto the most inferior end of G3, consistent with the connectivity profile of the subiculum, whereas ventral attention and somatomotor networks had a stronger medial position along G3, aligning with reported connectivity of CA1-3 (Figure 1D).

To elucidate the complimentary roles of gradients for behavior we linked their cortical patterns to the established macroscale layout of cortical function[48] using Spearman's rank correlation analyses. G1 showed significant correspondence with the cortical representation-modulation gradient[48,83], differentiating the DMN and somatomotor networks from attentional and control areas of the multiple-demand network[84,85] (left G1: Spearman's r = -0.353, p_{spin} < 0.001; right G1: Spearman's r = -0.406, p_{spin} < 0.001; Figure 1E). G1's correlation with this cortical gradient was greater than its correlations to other cortical gradients

($6.3 < Z < 9.6$, *ps* < 0.001), as well as significantly stronger than correlations observed for G2 and G3 ($1.6 < Z < 6.5$, *ps* < 0.05). In contrast, G2 corresponded to the principal unimodal-transmodal gradient of cortical function (left G2: Spearman's $r = 0.502$, $p_{spin} < 0.001$; right G2: Spearman's $r = 0.536$, $p_{spin} < 0.001$; Figure 1E), to a greater extent than G1 and G3 ($4.9 < Z < 10.9$, *ps* < 0.001) and in comparison to other cortical gradients ($5.2 < Z < 9.4$, *ps* < 0.001). Finally, the cortical pattern of G3 showed overall weaker correspondence with the canonical cortical gradients. G3's correlations with the unimodal-transmodal gradient (left G3: Spearman's $r = -0.32$, $p_{spin} = 0.011$), and the representation-modulation gradient (right G3: Spearman's $r = 0.191$, $p_{spin} = 0.009$), were significantly weaker compared their counterparts of G2 ($Z_{(998)} = 4.9$, $p < 0.001$) and G1 ($Z_{(998)} = 5.3$, $p < 0.001$). Taken together, multiple lines of converging evidence suggest that G1 and G2 serve as local maps of distinct macroscale axes of cortical organization.

Distinct patterns of behavioral transitions along G1 and G2

Given the correspondence of G1 and G2 to distinct gradients of cortical function, we characterized their relevance for hippocampal functional specialization by mapping transitions in behavioral domains onto G1 and G2 using meta-analytical decoding in Neurosynth[86]. Correlations were assessed between meta-analytical maps of behavioral terms and twenty-percentile bins of each gradient's cortical projection (Figure 2). First, a selection of terms commonly linked to anteroposterior hippocampal functional specialization[20,21] were assessed across G1 and ranked based on their location along the gradient (Figure 2A). This revealed an overarching verbal/social-to-spatial/cognitive axis. Terms that expressed the strongest anterior loadings on G1 included *words*, *social*, *recognition*, and *dementia*, whereas terms of *navigation*, *episodic memory*, *encoding* and *recollection* showed preferential posterior loadings. In contrast, behavioral transitions along G2 were expected to correspond to a perceptual/motor-associative

axis, given its unimodal-transmodal organization (Figure 1C-E). Terms were selected and ordered based on a previous report demonstrating transitions along a unimodal-transmodal cortical axis[48]. This separated *sensorimotor* and *visual* terms at one end from *social*, *self-referential*, and *default* terms at the other (Figure 2B).

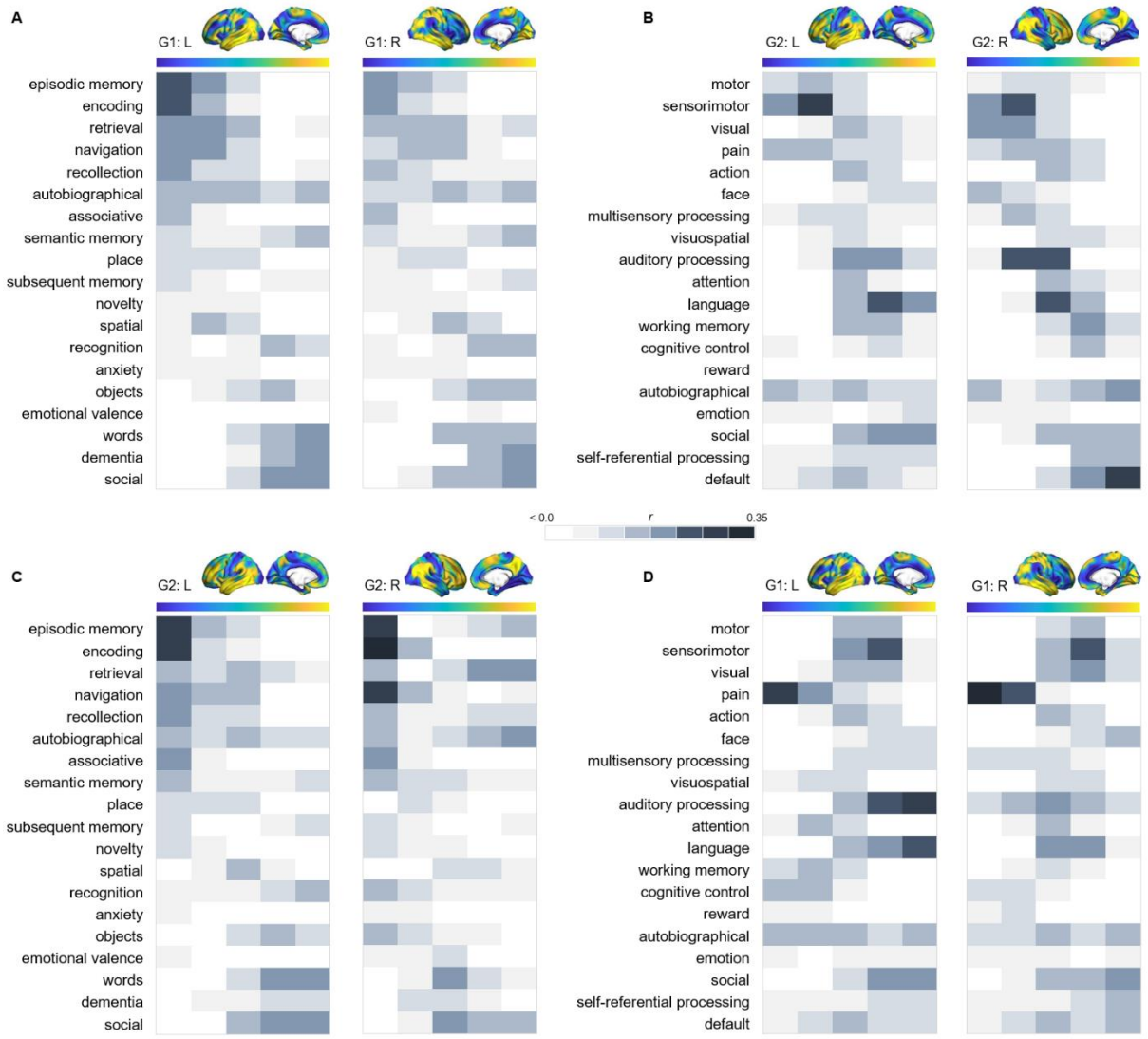

Figure 2. Behavioral profiling of G1 and G2. For each gradient, columns represents twenty-percentile bins of that gradient's cortical projection. Color shadings represent the strength of correlations between gradient bins and meta-analytical maps in Neurosynth. A) Terms commonly linked to anteroposterior hippocampal functional specialization were assessed across G1 and ranked based on their location along the gradient. This revealed an overarching verbal/social-to-spatial/cognitive axis, most evident across G1 in the left hemisphere. B) For G2, terms were selected and ordered based on a previous report demonstrating behavioral transitions along a unimodal-transmodal cortical axis[48]. C) The correspondence between G2 and behavioral terms commonly linked to anteroposterior hippocampal functional specialization. D) The correspondence between G1 and behavioral terms expressing a unimodal-transmodal axis.

Topography of G2 reflects distribution of hippocampal dopamine D1 receptors

Given the important modulation of hippocampal function by DA[57,58], we tested the spatial correspondence between functional gradients and the distribution of hippocampal DA receptors, focusing on the receptor subtype most abundantly expressed across cortex, D1DR, measured by [^{11}C]SCH23390 PET in the DyNAMiC sample. To estimate individual differences in gradient topography, trend surface modelling (TSM) was applied to each subject-level connectopic map[53,77]. This spatial-statistics approach parameterizes gradients at subject level, yielding a set of spatial model parameters which describe the topographic characteristics of each gradient in x, y, z directions (Supplementary Figure 4). Individual maps of D1DR binding potential were similarly submitted to TSM yielding a set of spatial model parameters describing the topographic characteristics of hippocampal D1DR distribution for each participant. D1DR parameters were subsequently used as predictors of gradient parameters in a multivariate GLM (controlled for age, sex, and mean FD). Individual differences in D1DR topography significantly explained topography of right-hemisphere G2 ($F = 1.207$, $p = 0.041$; partial $\eta 2 = 0.118$), but not of G1 nor G3 (F 0.902-1.108, *p* 0.222-0.750) (Figure 3). This association was robust across multiple TSM model orders (Supplementary Figure 5).

Moreover, we assessed gradients in relation to additional DA markers at group-level. To that end, a map of D1DR distribution was formed by averaging the [^{11}C]SCH23390 BP images across DyNAMiC participants (n=176), and a map of D2DR distribution was formed by averaging [^{11}C]raclopride BP images in a subsample of DyNAMiC participants (n = 20). Previously published maps of DAT[87] and FDOPA (https://www.nitrc.org/projects/spmtemplates) were also analyzed. Correlations across group-level TSM parameters[88], revealed significant positive associations between G2 and D1, DAT and FDOPA (D1: $r = 0.501$, $p < 0.01$; DAT: $r = 0.378$, $p < 0.01$; FDOPA: $r = 0.584$, $p < 0.01$; Figure 3C), although not D2 (D2: $r = 0.131$, $p = 0.44$), whereas correlations were not significant

for G1 or G3, indicating that G2 best captures shared principles of functional and neuromolecular brain organization.

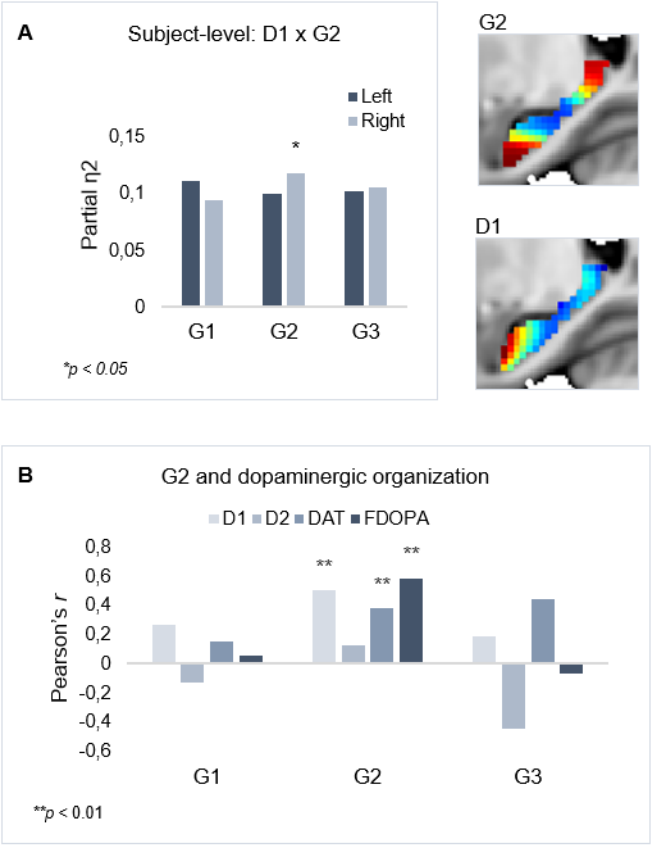

Figure 3. Shared functional and neuromolecular organization within the hippocampus. A) Multivariate effects of hippocampal D1DR TSM parameters as predictors of G2 TSM parameters. Images show average organization of G2 and D1DR in the right hemisphere. Note that the arbitrary color scale of G2 has been flipped. B) Correlations between group-level TSM parameters of functional gradients and DA markers.

Dedifferentiated gradient topography in older age

Age-related differences in gradient topography were assessed using multivariate GLMs including age as the predictor and gradient TSM parameters as dependent variables (controlling for sex and mean frame-wise displacement; FD). There was a significant effect of age on topographic characteristics of all three gradients. G1 displayed the greatest effect of age (left: $F_{(9,150)} = 5.853$, $p < 0.001$, partial $\eta^2 = 0.260$; right: $F_{(9,150)} = 6.971$, $p < 0.001$, partial $\eta^2 = 0.298$), followed by G2 (left: $F_{(12,147)} = 2.583$, $p = 0.004$, partial $\eta^2 = 0.174$; right: $F_{(12,145)} = 2.635$, $p = 0.003$, partial $\eta^2 = 0.179$), and G3 (left: $F_{(12,147)} = 1.973$, $p = 0.030$, partial $\eta^2 = 0.139$; right: $F_{(12,145)} = 2.082$, $p = 0.021$, partial $\eta^2 = 0.147$). To visualize effects, subject-level gradient values were plotted along the anteroposterior axis, averaged within groups of young (20-39

years), middle-aged (40-59 years) and older (60-79 years) adults (Figure 4A). Connectivity across G1 and G2 displayed less distinct differentiation at older age, depicted by the flatter curves in the older group (Figure 4A).

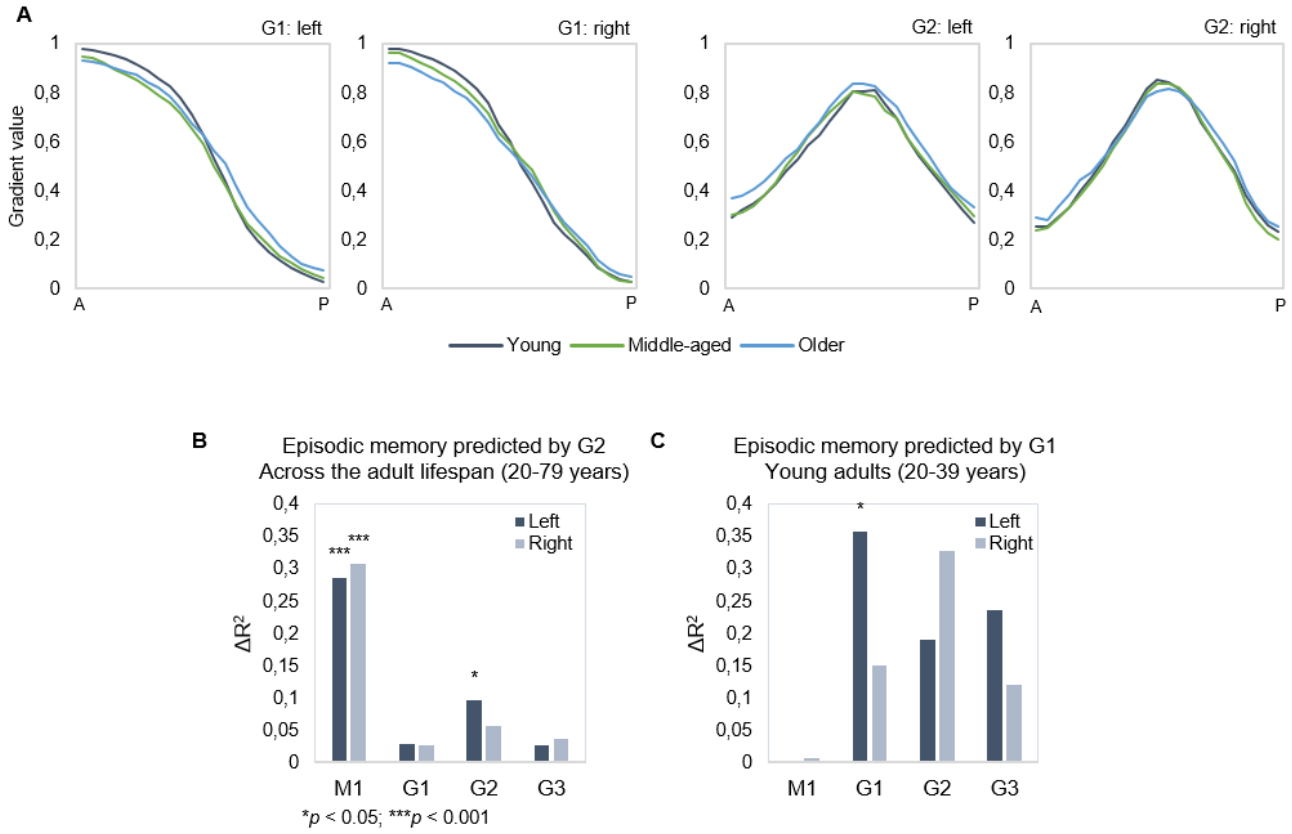

Figure 4. Hippocampal gradients in relation to age and episodic memory. A) Less specificity in connectivity change across gradients in older age. Average values of subject-level G1 and G2 bins (~2mm) plotted as a function of their distance (in mm) from the most anterior hippocampal voxel. Separate lines are displayed for young (20-39 years; gray), middle-aged (40-59 years, green), and older (60-79 years; blue) age groups. The flatter curves in the older group indicate less distinct change in connectivity patterns across gradients in older age. B) Individual differences in topographic characteristics of left-hemisphere G2 significantly predicted episodic memory performance across the sample, over and above the first- and second-step models (M1: age, sex, in-scanner motion; G1 parameters). C) Topographic characteristics of G1 in the left hemisphere significantly predicted episodic memory performance in young adults, over and above M1 (age, sex, and in-scanner motion).

Topography of hippocampal gradients predicts episodic memory performance

Next, we investigated the relationship between individual differences in gradient topography and episodic memory. Using hierarchical multiple regression models, in which age, sex, and

mean FD were controlled for in a first step (M1), we entered TSM parameters of the three gradients as predictors of episodic memory in a step-wise manner. Models were assessed separately for left and right hemispheres. Memory performance was, across the sample, significantly predicted by individual differences in G2 topography in the left hippocampus (Adj. R^2 = 0.308, ΔR^2 = 0.096, F= 1.842, *p* = 0.047) over and above covariates and topography of G1, which did not predict performance (Adj. R^2 = 0.260, ΔR^2 = 0.029, F= 0.695, *p* = 0.713), and neither did G3 (Adj. R^2 = 0.276, ΔR^2 = 0.027, F= 0.502, *p* = 0.910), Figure 4B. Memory performance was, within young adults, predicted by left-hemisphere G1 topography (Adj. R^2 = 0.182, ΔR^2 = 0.357, F= 2.672, *p* = 0.015), whereas neither G2 (Adj. R^2 = 0.204, ΔR^2 = 0.191, F= 1.098, *p* = 0.396) nor G3 (Adj. R^2 = 0.384, ΔR^2 = 0.236, F= 1.755, *p* = 0.132) significantly improved the prediction (Figure 4C). No gradient predicted memory within middle-aged or older age groups (F 0.432-1.865, *p* 0.928-0.113; Supplementary Table 1).

Youth-like gradient topography supports memory in older age

To investigate the functional role of G1 in old age, the principal and most age-sensitive gradient, we tested whether mnemonic functioning in older adults would be facilitated by youth-like gradient topography, using two independent datasets. In DyNAMiC, we applied data-driven latent class analysis (LCA) to TSM parameters (residualized to account for age, sex, and mean FD) of left-hemisphere G1, which predicted episodic memory performance in younger adults. LCA yielded a two-class solution identifying two subgroups (n=19 vs. n=30) of older adults (60-79 years), which by definition differed in left-hemisphere G1 characteristics ($F_{(9,37)}$ = 13.778, *p A*< 0.001, partial η^2 = 0.770). A difference was also evident in the right hemisphere ($F_{(9,37)}$ = 3.790, *p* = 0.002, partial η^2 = 0.480).

Individuals in the smaller subgroup were determined as exhibiting an aged gradient profile, whereas older adults in the larger subgroup as exhibiting a youth-like gradient

profile. The classification based on G1 parameters extended across all three gradients in both hemispheres (Figure 5A), such that the smaller sub group displayed marked differences from younger adults across all gradients (left G1: $F_{(9,63)} = 15.549$, $p < 0.001$, partial $\eta^2 = 0.690$; right G1: $F_{(9,63)} = 5.322$, $p < 0.001$, partial $\eta^2 = 0.432$; left G2: $F_{(12,60)} = 3.991$, $p < 0.001$, partial $\eta^2 = 0.444$; right G2: $F_{(12,60)} = 2.192$, $p = 0.023$, partial $\eta^2 = 0.305$; left G3: $F_{(12,60)} = 2.832$, $p = 0.004$, partial $\eta^2 = 0.362$; right G3: $F_{(12,60)} = 1.844$, $p = 0.061$, partial $\eta^2 = 0.269$), while the youth-like sub group differed less from young adults in terms of G1 (left G1: $F_{(9,74)} = 4.416$, $p < 0.001$, partial $\eta^2 = 0.349$; right G1: $F_{(9,74)} = 3.086$, $p = 0.003$, partial $\eta^2 = 0.273$), and displayed second- and third-order gradients comparable to those in younger age (left G2: $F_{(12,71)} = 1.616$, $p = 0.107$, partial $\eta^2 = 0.215$; right G2: $F_{(12,71)} = 1.442$, $p = 0.168$, partial $\eta^2 = 0.196$; left G3: $F_{(12,71)} = 1.122$, $p = 0.357$, partial $\eta^2 = 0.159$; right G3: $F_{(12,71)} = 1.596$, $p = 0.112$, partial $\eta^2 = 0.212$). Classification of older adults based on right-hemisphere G1 is presented in the Supplementary Information (Supplementary Figure 6).

By examining the change in connectivity along G1 and G2 in the aged and youth-like subgroups, we found that the diminished topographic specificity observed across gradients in older individuals was primarily driven by older adults displaying an aged gradient profile (Figure 5B). Both older subgroups displayed altered gradient organization across cortex (Figure 5C-D). The distribution of cortical networks in G1 space indicated a unimodal-transmodal organization in youth-like older adults, not evident in the aged older group (Figure 5D). The two groups did not differ in terms of age (aged: 70.8±6.0; youth-like: 68.4±4.7; $t = 1.548$, $p = 0.128$), sex (aged: 9 men/10 women; youth-like: 16 men/14 women; $X^2 = 0.166$, $p = 0.684$), nor hippocampal gray matter (left hemisphere: aged: 4271.2±480.9; youth-like: 4246.8±269.1; $t = 0.223$, $p = 0.824$; right hemisphere: aged: 3866.2±446.3; youth-like: 3979.9±398.1; $t = 0.929$, $p = 0.357$). In line with our hypothesis, we observed superior memory in older adults exhibiting a youth-like gradient profile (Figure 5E): at trend-level for the composite episodic measure

(aged: 43.2±3.7; youth-like: 46.5±6.6; t = 1.958, p = 0.056), driven by a significant group difference on its word recall sub test (aged: 40.9±4.5; youth-like: 43.4±6.8; t = 2.600, p = 0.012). Word recall performance was furthermore predicted by left-hemisphere G1 parameters (over and above age, sex, and mean FD) in the youth-like older adults (Adj. R^2 = 0.464, ΔR^2 = 0.543, F = 3.043, p = 0.028), while no such association was observed in the aged older sub group (Adj. R^2 = 0.063, ΔR^2 = 0.533, F = 1.004, p = 0.518).

We similarly identified two classes of older adults in the Betula sample, through LCA based on TSM parameters describing the topography of left-hemisphere G1 (class 1: n = 60; class 2: n = 99; $F_{(9,149)}$ = 35.993, p < 0.001, partial η^2 = 0.685, Supplementary Figure 6). A difference in gradient topography between classes was also evident for G1 in the right hemisphere ($F_{(9,149)}$ = 2.134, p = 0.030, partial η^2 = 0.114). The smaller class was, in relation to young adults, determined as exhibiting an aged G1 ($F_{(9,63)}$ = 4.166, p < 0.001, partial η^2 = 0.373) in contrast to the bigger class displaying a more youth-like G1 ($F_{(9,102)}$ = 1.345, p = 0.223, partial η^2 = 0.106). Importantly, we observed a trend-level difference in word recall performance between subgroups ($t_{(157)}$ = 1.585, p = 0.058, 1-tailed), such that youth-like older adults displayed superior memory performance (Supplementary Figure 6).

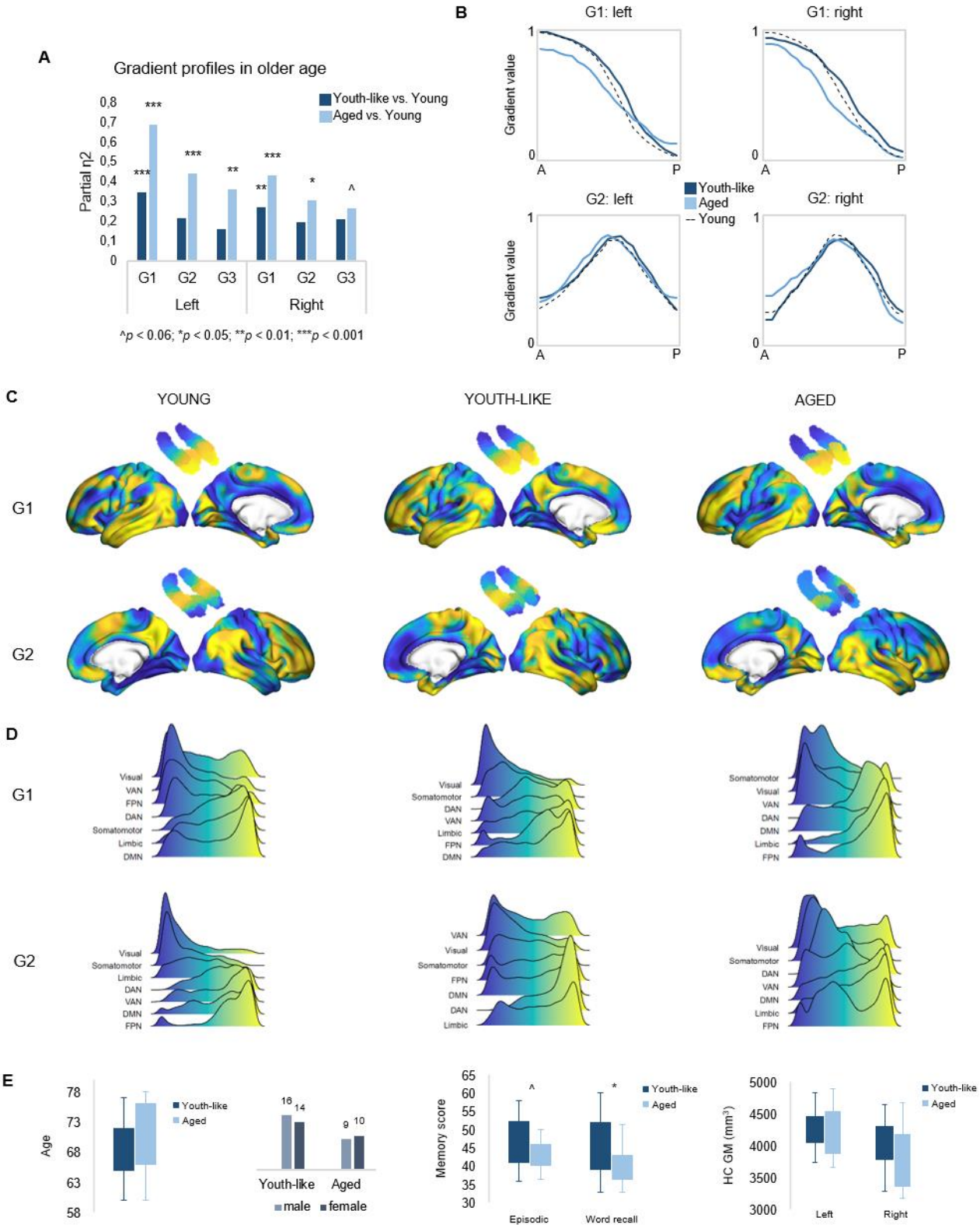

Figure 5. Gradient profiles in older age. A) Two older sub groups were identified based on left-hemisphere G1. The first group (n=19) displayed gradient characteristics significantly different from those in young adults, whereas the second group (n=30) displayed gradient characteristics more similar to those in young adults. Bars represent comparisons of gradient TSM parameters between older sub groups and younger adults. B) Average gradient values across participants within sub groups, plotted against the distance (in mm) from the most anterior hippocampal voxel. The flatter curves in older adults with an aged gradient profile suggest less distinct change in connectivity across gradients. C) Group-

level G1 and G2 for young, youth-like, and aged groups. D) Position of cortical networks in gradient space. E) Older sub groups were comparable in terms of age, sex, and hippocampal gray matter volume, while older adults with a youth-like gradient profile exhibited higher episodic memory performance.

Discussion

In this study, we present a comprehensive multidimensional characterization of functional hippocampal-cortical integration across the adult human lifespan, and meticulously map topography of connectivity gradients onto behavioral and neuromolecular phenotypes. Our findings reveal the presence of two distinct connectivity gradients distributed along the hippocampus longitudinal axis which significantly contribute to inter-individual differences in episodic memory. Critically, we demonstrate that a youth-like gradient profile in older age, characterized by maintained distinctiveness of connectivity change along gradients, is linked to superior mnemonic function. This highlights loss of specificity in gradient topography as a potential hippocampal marker of memory decline in aging. Our results underscore the necessity of disentangling multiple dimensions of hippocampal functional organization to advance the understanding of cortico-hippocampal systems involved in memory and behavior.

Gradient mapping has emerged as a powerful alternative to traditional parcellation-based approaches to functional connectivity, which are typically unable to tease apart overlapping modes of function within a brain region. Here, connectopic mapping[77] in two independent samples revealed a principal hippocampal gradient, G1, of anteroposterior change in cortical connectivity, aligning well with previous gradient-based observations in young adults[50–53]. A second-order gradient, G2, conveyed long-axis change in connectivity separating the middle hippocampus from anterior and posterior ends, while a third-order gradient, G3, conveyed variation across the hippocampus transverse axis. Although we restrict our discussion of G3 given its low proportion of explained variance, we note that it mirrors patterns previously observed in both structure and function[20,89], at a coarse scale separating CA areas from the subiculum. Consistently, cortical patterns of this gradient matched cortical connectivity profiles

previously reported for hippocampal subfields[27,51,82]. Although our results underscore the notion that function favors detection of anteroposterior hippocampal organization, in contrast to that determined by its cytoarchitecture[34], they indicate that higher-order connectivity modes may indeed carry coarse-scale information about subfield-determined organization.

Importantly, our results reveal a framework of cortico-hippocampal integration in which the DMN is positioned in different neural contexts: in one case at the opposite end from frontoparietal networks of attention and control, and in the other, opposite to sensorimotor and visual networks – indicating that an account of the hippocampus' functional connectivity with the DMN is dependent on multiple neurofunctional hierarchies. Across cortex, G1 reflected a pattern corresponding to the representation-modulation gradient of cortical function (Figure 1C-E)[48], traditionally also termed task-positive/task-negative[90], which highlights areas of the multiple demand network[84,85] by separating frontoparietal areas of attention and control from sensorimotor and DMN areas. Using meta-analytical decoding in Neurosynth, we observed behavioral transitions that describe G1 as a bridge between self-centric, affective, and social – in contrast to – world-centric and cognitive poles[20,31]. While our meta-analytical results are descriptive, task-positive terms such as navigation, episodic memory, encoding and recollection, as well as attention and cognitive control, mapped on to the posterior end of the gradient, whereas verbal and social terms showed preferential mapping onto the anterior section of the gradient (Figure 2). In parallel to G1, the distribution of cortical networks in gradient space, transitions in meta-analytical terms, and spatial correlations with gradients of macroscale cortical organization, determined G2 as a local representation of the principal unimodal-transmodal cortical gradient (Figure 1C-E), evident across a wide range of functional, structural and molecular modalities[47–49,91,92]. Specifically, recent evidence from our group and others describe the distribution of postsynaptic D1DR across cortex as following a unimodal-transmodal axis[69,70]. Given that DA neurotransmission plays a key role in hippocampus-

dependent function, and influences the brain's functional architecture by synaptic modulation[58,59], we tested whether the topography of hippocampal gradients reflected the underlying distribution of D1DR. Observing topographic correspondence between G2 and several DA markers (Figure 3B), we suggest that G2 may constitute a functional mode of the hippocampus reflecting a dopaminergic phenotype.

The overlap of G1 and G2 may potentially reflect the superimposition of gradients and hubs of long-axis anatomical connections indicated in both the human and animal hippocampus[29,33]. Moreover, the observation that macroscale relationships between distinct cortical systems are mapped out by the hippocampus may reflect its primordial position in the laminar differentiation characterizing the development of the cerebral cortex[93,94]. This supports the notion that the functional organization of the hippocampus stands, from a phylogenetic perspective, to inform general principles of brain organization[34,83].

Insight into how these distinct organizational gradients of hippocampal function potentially alter in aging and collectively contribute to memory function, however, remains limited, as previous studies use younger samples and rarely estimate inter-individual differences in gradient topography[50–53]. Here, trend-surface modelling allowed for parameterization of gradients at subject level and thereby estimation of inter-individual differences[53,77]. Whereas topography of G1 predicted episodic memory in young adults, consistent with one previous study[53], results support a primary role of the less known G2 in episodic memory across the adult lifespan. Meta-analytical decoding of G2 primarily described the unimodal connectivity patterns of the anterior and posterior hippocampus as linked to memory-related terms (Figure 2C). G2's role in memory might as such be considered in light of hippocampal integration with the ventral visual system, by which it contributes to complex perceptual processes supporting memory[95,96]. In humans, there is evidence of direct hippocampal connections to early visual areas[97,98], with recent tractography-based work

demonstrating connectivity endpoints as primarily localized to the posterior hippocampus and to a smaller region in the anterior hippocampus[33].

It is noteworthy that G1 and G2 displayed comparable organization across the adult lifespan, although significant age-related variation in their fine-scale topography was evident (Figure 4). Older age was associated with less distinct change in connectivity along G1 and G2, an effect that was exacerbated in a sub group of older adults identified as exhibiting an aged gradient profile, separated from older adults exhibiting youth-like gradient topography through classification based on gradient parameters (Figure 5A). This finding constitutes a novel addition to a growing body of evidence highlighting increased homogeneity in hippocampal function in aging[76,99]. Current theories view increased functional homogeneity of the hippocampus as a consequence of its functional isolation from cortical areas, arising from tau-driven degeneration of the perforant pathway[76,100,101]. Constituting the main source of input to the hippocampus, age-related deterioration of this pathway has previously been demonstrated as leading to impaired mnemonic functioning[102,103]. In two independent samples, we showed that older individuals with an aged gradient profile, but comparable hippocampal volumes, showed less efficient episodic memory compared to older individuals with youth-like gradient topography (Figure 5 and Supplementary Figure 6). These findings underscore the potential of gradient mapping to capture aberrant alterations in hippocampal function at an early stage.

Altered organization of G1 across cortex was evident in both older sub groups, consistent with the loss of segregation between task-positive and task-negative poles generally observed in older adults[60,104–107]. Such neural dedifferentiation is also evident in numerous psychiatric diseases involving hippocampal dysfunction[108,109], like major depression[110,111], schizophrenia[112], and Alzheimer's disease[113]. Consistently, functional maintenance of the multiple demand network has been linked to preserved cognition in aging[114]. There was, however, a main difference in deviation from this cortical pattern observed between older sub

groups, such that a unimodal-transmodal organization was evident in youth-like older adults, whereas not in the aged older group (Figure 5D). A meaningful role of this difference is indicated by the observation that individual differences in topography of G1 predicted episodic memory in youth-like older adults only.

Whereas longitudinal data is required to inform the underlying mechanisms of individual differences and maintenance of hippocampal gradient topography in older age[115,116], our results motivate further evaluation of hippocampal gradient topography as a potential marker of cognitive decline. Furthermore, whereas connectopic mapping[77,117] allows for subject-level parameterization of gradients through spatial statistical modelling, there is currently limited means for statistical inference across the cortical projections of gradients. As such, there is a descriptive quality to some aspects of this study, although thorough measures have been taken to evaluate characteristics of cortical motifs from multiple perspectives. Importantly, gradients showed high correspondence with available previous observations, and were reproduced in an independent data set, as well as in a sub group of younger participants.

This study presents two overlapping modes of functional connectivity organized along the hippocampal longitudinal axis. The understanding of these as local manifestations of distinct and complementary large-scale neocortical motifs marks a significant advancement in the understanding of hippocampal functional organization. The topography of the two long-axis modes were linked to episodic memory, and revealed shared principles of functional and neuromolecular organization within the hippocampus. Collectively, our results provide a multidimensional framework for understanding hippocampal cortical integration and its contribution to memory across the adult human lifespan.

Methods

This study included data from the DopamiNe, Age, connectoMe, and Cognition (DyNAMiC) study, for which the design and procedures have been described in detail elsewhere[78]. Here, we include the materials and methods relevant to the current study. DyNAMiC was approved by the Regional Ethical board and the local Radiation Safety Committee of Umeå, Sweden. All participants provided written informed consent prior to testing.

Participants

The DyNAMiC sample included 180 participants (20-79 years; mean age = 49.8±17.4; 90 men/90 women equally distributed within each decade). Individuals were randomly selected from the population register of Umeå, Sweden, and recruited via postal mail. Exclusion criteria implemented during the recruitment procedure included brain pathology, impaired cognitive functioning (Mini Mental State Examination < 26), medical conditions and treatment that could affect brain functioning and cognition (e.g. dementia, diabetes, and psychiatric diagnosis), and brain imaging contraindications (e.g. metal implants). All participants were native Swedish speakers. A total of 16 participants were excluded from connectopic mapping due to excessive in-scanner motion, leaving resting-state fMRI data for 164 participants (20-78 years; mean age = 48.7±17.3). As a replication data set, we used an independent sample of 224 cognitively healthy and native Swedish-speaking adults (122 men/102 women; 29-85 years mean age = 65.0±13.0) from the population-based Betula project, for which the design and recruitment procedures have been reported in detail elsewhere[79,80].

Episodic memory

Episodic memory was measured using three tasks testing word recall, number-word recall and object-location recall, respectively[78,118]. In the word recall task, participants were presented

with 16 Swedish concrete nouns that appeared successively on a computer screen. Each word was presented for 6 s during encoding with an inter-stimulus interval (ISI) of 1 s. Following encoding, participants reported as many words as they could recall by typing them using the keyboard. Two trials were completed, yielding a maximum score of 32. In the number-word task, participants encoded pairs of 2-digit numbers and concrete plural nouns (e.g., 46 dogs). During encoding, eight number-word pairs were presented, each displayed for 6 s, with an ISI of 1 s. Following encoding, nouns were presented again, in a re-arranged order, and participants had to report the 2-digit number associated with each presented noun (e.g. How many dogs?). This task included two trials with a total maximum score of 16. The third task was an object-location memory task. Here, participants were presented with a 6 × 6 square grid in which 12 objects were, one by one, shown at distinct locations. Each object-position pairing was displayed for 8 s, with an ISI of 1 s. Following encoding, all objects were simultaneously shown next to the grid for the participant to move them (in any order) to their correct position in the grid. If unable to recall the correct position of an object, participants had to guess and place the object in the grid to the best of their ability. Two trials of this task were completed, making the total maximum score 24.

A composite score of performances across the three tasks was calculated and used as the measure of episodic memory. For each of the three tasks, scores were summarized across the total number of trials. The three resulting sum scores were z-standardized and averaged to form one composite score of episodic memory performance (T score: mean = 50; SD = 10). Missing values were replaced by the average of the available observed scores.

Image acquisition

Brain imaging was conducted at Umeå University Hospital, Sweden. Structural and functional MRI data were acquired with a 3T Discovery MR 750 scanner (General Electric, WI, USA),

using a 32-channel head coil. Positron emission tomography (PET) data were acquired with a Discovery PET/CT 690 scanner (General Electric, WI, USA).

Structural MR Imaging

Anatomical T1-weighted images were acquired with a 3D fast-spoiled gradient-echo sequence, collected as 176 slices with a thickness of 1 mm. Repetition time (TR) was 8.2 ms, echo-time (TE) = 3.2 ms, flip angle = 12º, and field of view (FOV) = 250 × 250 mm.

Functional MR Imaging

Functional MR data were collected during resting-state, with participants instructed to keep their eyes open and focus on a fixation cross during scanning. Images were acquired using a T2*-weighted single-shot echo-planar imaging (EPI) sequence, with a total of 350 volumes collected over 12 minutes. The functional time series was sampled with 37 transaxial slices, slice thickness = 3.4 mm, and 0.5 mm spacing, TR = 2000 ms, TE = 30 ms, flip angle = 80º, and FOV = 250 x 250 mm. Ten dummy scans were collected at the start of the sequence.

PET Imaging

PET was conducted in 3D mode with a Discovery PET/CT 690 (General Electric, WI, US) to assess whole-brain dopamine D1 receptor availability using the radioligand [^{11}C]SCH23390. Scanning was done during a resting condition, with participants instructed to lay still and remain awake with their eyes open. To minimize head movement, a thermoplastic mask (Posicast®; CIVCO medical solutions; IA, US) was individually fitted for each participant, and attached to the bed surface during scanning. Following a low-dose CT scan (10 mA, 120 kV, and 0.8 s rotation time) for attenuation correction, an intravenous bolus injection with target radioactivity of 350 MBq [^{11}C]SCH23390 was administered. The PET scan was a 60 min dynamic scan, with 6 x 10 s, 6 x 20 s, 6 x 40 s, 9 x 60 s, 22 x 120 s frames. The average radioactivity dose

administered to participants was 337±27 MBq (range 205-391 MBq). Due to participant drop-out and technical issues, complete PET data was available for 177 DyNAMiC participants.

Image preprocessing

Hippocampal segmentation and volumetric assessment

Individual anatomical T1-weighted images were submitted to automated segmentation in FreeSurfer version 6[119,120]. A mean image of participants' normalized T1-weighted images was also segmented in FreeSurfer, and yielded hippocampal and cortical segmentations used as masks for connectopic mapping. Regional gray matter (GM) volume was estimated from subject-specific hippocampal segmentations, and were corrected for total intracranial volume (ICV; the sum of volumes for grey matter, white matter, and cerebrospinal fluid). Adjusted volumes were equal to the raw volume - *b*(ICV - mean ICV), where *b* is the regression slope of volume on ICV[121,122]. Automated segmentation of the hippocampus into subiculum, CA1-3, and DG/CA4 subfields was conducted in FreeSurfer using the group-average T1-weighted image, for sample-specific masks to overlay onto G3.

Functional MRI data

Resting-state fMRI data were preprocessed using Statistical Parametric Mapping (SPM12: Wellcome Trust Centre for Neuroimaging, http://www.fil.ion.ucl.ac.uk/spm/) implemented in an in-house software, DataZ. Functional images were slice-timing corrected, co-registered to the anatomical T1-images, and motion corrected, and underwent distortion correction using subject-specific B0-field maps. The functional data were subsequently co-registered to the anatomical T1-images again, temporally demeaned and linear and quadratic effects were removed. Next, a 36-parameter nuisance regression model was applied[123], including mean cerebrospinal, white-matter, and whole-brain signal in addition to six motion parameters, including parameters' squares, derivatives, and squared derivatives. To further control for in-

scanner motion, the model also included a set of spike regressors, defined as binary vectors of motion-contaminated volumes exceeding a volume-to-volume root-mean-squared (RMS) displacement of 0.25 mm[124]. A temporal high-pass filter (with a threshold of 0.009 Hz) was applied simultaneously as nuisance regression in order to not re-introduce nuisance signals[125]. Finally, images were normalized to MNI space by Diffeomorphic Anatomical Registration using Exponentiated Lie algebra (DARTEL: Ashburner, 2007) and smoothed with a 6-mm FWHM Gaussian kernel. Four individuals were excluded from the template-generation step due to non-pathological anatomical irregularities. In total, 16 participants were excluded due to displaying excessive in-scanner motion, as defined by displaying i) more than 20 volumes with >0.25 relative RMS difference in motion, and ii) greater than 0.2 average RMS across the run. On average, the relative RMS difference in motion across the sample was 0.090 (± 0.063), and the mean frame-wise displacement (FD) was 0.164 (± 0.104).

Dopamine D1 receptor availability

Preprocessing of PET data was performed in SPM12 (Wellcome Trust Centre for Neuroimaging, http://www.fil.ion.ucl.ac.uk/spm/). Binding potential relative to non-displaceable binding in a reference region (BP_{ND}; Innis et al., 2007), was used as an estimate of receptor availability (i.e. D1DR) in the hippocampus, for each participant defined using the FreeSurfer segmentation of their anatomical images. Cerebellum was used as reference region. PET images were corrected for head movement by using frame-to-frame image co-registration, and co-registered with T1-weighted MRI images with re-slicing to T1 voxel size. The simplified reference-tissue model (SRTM) was used to model regional time-activity course (TAC) data[128]. Regional TAC data were adjusted for partial volume effects (PVE) by using the symmetric geometric transfer matrix (SGTM) method implemented in FreeSurfer[129], and an estimated point-spread-function of 2.5 mm full-width-at-half-maximum (FWHM). We additionally used data from a publicly available database of group-averaged volumetric maps of molecular target

distributions (https://github.com/netneurolab/hansen_receptors). Specifically, we downloaded previously published maps of DAT[87] and FDOPA (https://www.nitrc.org/projects/spmtemplates), to investigate the spatial correspondence between functional gradients and dopaminergic target distributions.

Mapping gradients of functional connectivity

Connectopic mapping[77] was run through the ConGrads toolbox[77,117] implemented in FSL[130,131]. Mapping was conducted on both subject level and group level, for the left and right hippocampus separately, and involved two main steps. First, for every hippocampal voxel, connectivity fingerprints were computed as the Pearson correlation between the voxel-wise time-series and a singular-value decomposition (SVD) representation of all cortical voxels. In a second step, non-linear manifold learning (Laplacian eigenmaps) was applied to a matrix expressing the degree of similarity between the voxel-wise fingerprints. This yields eigenvectors, so called connectopic maps, representing modes of functional connectivity (i.e. functional gradients). Each connectopic map is then projected onto cortex, for which each vertex is color coded according to the voxel in the hippocampus it correlates the most with. Since connectopic mapping at group level involves applying Laplacian eigenmaps to a group-average similarity matrix, group level mapping across the sample was conducted using the hippocampal and cortical masks derived from the FreeSurfer segmentation of a sample-mean structural image. Mapping was specified to compute 20 gradients, and a subsequent scree plot over explained variance indicated meaningful contributions of the three first connectopic maps, together explaining 67% of the variance across hemispheres (Supplementary Figure 1).

Alignment of connectopic maps across participants

To ensure optimal alignment of identified connectopic maps across participants, we employed Procrustes alignment, based on voxel-wise correlations, to order subject-level connectopic

maps according to their correspondence with a set of reference maps (i.e. gradients computed at group level across the full sample). Moreover, whereas the sign of connectopic maps is arbitrary, differences therein have an impact on the spatial model parameters describing the topographic characteristics of gradients, derived through TSM in a later step. As such, the sign of subject-level connectopic maps showing negative correlations with the corresponding group-level reference map were inversed.

Trend surface modelling

Using spatial statistics, the topography of a connectopic map can be represented by a small number of spatial model parameters. This parameterization enables analyses of inter-individual differences, and is achieved through trend surface modelling (TSM), implemented in a third step of the ConGrads analysis pipeline[77]. In this step, the spatial pattern of each subject-level connectopic map is approximated by estimating a spatial statistical model. Model estimation involves fitting a set of polynomial basis functions along canonical axes of the connectopic map. In MNI space, this entails estimation along x, y, and z axes of the hippocampus. Thus, fitting a polynomial of degree 1 yields three TSM parameters (x, y, z), with any increase in model order corresponding to an increase in number of parameters (e.g. 6 parameters for the second model order: x, y, z, x^2, y^2, z^2; 9 parameters for the third model order, etc.). Trend surface models are fitted with an increasing polynomial degree using Bayesian linear regression, which provides likelihood estimates that can be used for subsequent model selection. Here, model selection was based on three information sources: a) the Bayesian Information Criterion (BIC) across subjects for models estimated at orders 1-10; b) the % explained variance in connectopic maps by each model; and c) visual inspection of group-level gradients reconstructed from TSM parameters at different model orders. The purpose of using multiple information sources, as opposed to simply BIC, was to find a trade-off between high-quality reconstructions of gradients by TSM models, while keeping the number of model parameters sufficiently low for

multivariate statistical analyses. A model order of 3 (=9 TSM parameters) was selected for G1, whereas a model order of 4 (=12 TSM parameters) was selected for G2 and G3 (Supplementary Figure 5). Each gradient's set of TSM parameters were then used as either dependent or independent variables in multivariate GLMs investigating links between gradient topography and variables such as age, episodic memory performance, and D1DR distribution.

Transitions in connectivity as a function of the hippocampal longitudinal axis

To visualize the orthogonal patterns of change in connectivity conveyed by each gradient, and to aid in the interpretation of age effects, we divided each subject-level connectopic map into 23 bins of ~2mm along the hippocampus anterior-posterior axis and estimated the average gradient value (ranging from 0-1) for each bin. Plotting the values of each bin against their distance in mm from the most anterior voxel in the hippocampus as such demonstrates the pattern of change in connectivity along the anterior-posterior axis[53].

Cortical projections and correlations with gradients of cortical function

In ConGrads[77], cortical mapping is computed independently for each gradient based on the regression equation: $pmap = \boldsymbol{B^T}.(\boldsymbol{X^T}^{-1}.\boldsymbol{A^T})^T$ where A corresponds to data inside (i.e., hippocampus) and B to data outside (i.e., cortical) the ROI, and X-1 is the pseudo-inverse of the corresponding eigenvector (stacked with a row of ones). For each hippocampal gradient, the volumetric MNI-registered group-level cortical projection map was resampled to the Human Connectome Project 32k_LR midthickness surface mesh, using the volume-to-surface algorithm with enclosing mapping available in Connectome Workbench v.1.5.0[132]. Spearman correlations were computed between the cortical projection of each hippocampal gradient and the three gradients previously established as the main axes of cortical functional organization[48]. To reduce the degree of freedom, each surface projection was resampled by 1000-cortical parcels[133]. Statistical significance of correlations was assessed by spin-test permutation[134],

randomly rotating a spherical projection of the cortical maps 1000 times, with two-tailed statistical significance determined at a 95% confidence level.

Mapping behavioral transitions along gradients using Neurosynth

Transitions in behavioral domains were mapped onto G1 and G2 using meta-analytical decoding in Neurosynth[86]. We assessed two sets of behavioral terms (Figure 2), the first was a selection of terms commonly linked to anteroposterior hippocampal functional specialization[20,21], and the second a selection of terms based on a previous report demonstrating behavioral transitions along a unimodal-transmodal cortical axis[48]. For correspondence with meta-analytical maps, we created region of interest masks by projecting the cortical surface of each gradient to the 2-mm volumetric MNI152 standard space. These volumetric images were then divided into five twenty-percentile bins and binarized. The resulting images were used as input to the Neurosynth decoder, yielding an *r* statistic associated with each behavioral term per section of each gradient.

Acknowledgements

This work was supported by the Swedish Research Council (grant number 2016-01936 to A.S.), Riksbankens Jubileumsfond (grant number P20-0515 to A.S.), Knut and Alice Wallenberg Foundation (Wallenberg Fellow grant to A.S.), and StratNeuro grant at Karolinska Institutet (A.S.). The Betula Study is supported by a Scholar grant to L.N. from the Knut and Alice Wallenberg Foundation. FreeSurfer calculations were enabled by resources provided by the Swedish National Infrastructure for Computing (SNIC) at HPC2N, partially funded by the Swedish Research Council through grant agreement no. 2018-05973.

Author contributions

K.N., A.S., A.R, and F.G. conceived the study idea. F.F., M.A., J.J., R.P., A.A., and K.N. performed the data processing and formal analysis. All authors contributed to the interpretation of the findings. K.N. and A.S. wrote the manuscript with valuable feedback and revision by R.P., F.F., J.J., F.G., M.A., S.K., L.B., A.Z., A.R., and L.N.

References

1. Burgess, N., Maguire, E. A. & O'Keefe, J. The human hippocampus and spatial and episodic memory. *Neuron* **35**, 625–641 (2002).
2. Laurita, A. C. & Spreng, N. The Hippocampus and Social Cognition. in *The Hippocampus from Cells to Systems: Structure, Connectivity, and Functional Contributions to Memory and Flexible Cognition* (eds. Hannula, D. E. & Duff, M. C.) 537–558 (Springer International Publishing, 2017). doi:10.1007/978-3-319-50406-3_17.
3. Moscovitch, M., Cabeza, R., Winocur, G. & Nadel, L. Episodic memory and beyond: the hippocampus and neocortex in transformation. *Annu. Rev. Psychol.* **67**, 105–134 (2016).
4. Nadel, L. & Peterson, M. A. The hippocampus: Part of an interactive posterior representational system spanning perceptual and memorial systems. *J. Exp. Psychol. Gen.* **142**, 1242–1254 (2013).
5. Squire, L. R. Memory systems of the brain: A brief history and current perspective. *Neurobiol. Learn. Mem.* **82**, 171–177 (2004).
6. Eichenbaum, H. A cortical–hippocampal system for declarative memory. *Nat. Rev. Neurosci.* **1**, 41–50 (2000).
7. Ranganath, C. & Ritchey, M. Two cortical systems for memory-guided behaviour. *Nat. Rev. Neurosci.* **13**, 713–726 (2012).
8. Barnes, J. *et al.* A meta-analysis of hippocampal atrophy rates in Alzheimer's disease. *Neurobiol. Aging* **30**, 1711–1723 (2009).
9. Braak, H. & Braak, E. Neuropathological stageing of Alzheimer-related changes. *Acta Neuropathol. (Berl.)* **82**, 239–259 (1991).
10. Campbell, S. & MacQueen, G. The role of the hippocampus in the pathophysiology of major depression. *J. Psychiatry Neurosci.* **29**, 417–426 (2004).
11. Harrison, P. J. The hippocampus in schizophrenia: a review of the neuropathological evidence and its pathophysiological implications. *Psychopharmacology (Berl.)* **174**, 151–162 (2004).
12. Lieberman, J. A. *et al.* Hippocampal dysfunction in the pathophysiology of schizophrenia: a selective review and hypothesis for early detection and intervention. *Mol. Psychiatry* **23**, 1764–1772 (2018).
13. Xie, L. *et al.* Longitudinal atrophy in early Braak regions in preclinical Alzheimer's disease. *Hum. Brain Mapp.* **41**, 4704–4717 (2020).
14. Amaral, D. G. & Witter, M. P. The three-dimensional organization of the hippocampal formation: A review of anatomical data. *Neuroscience* **31**, 571–591 (1989).
15. Witter, M. P. & Amaral, D. G. The entorhinal cortex of the monkey: VI. Organization of projections from the hippocampus, subiculum, presubiculum, and parasubiculum. *J. Comp. Neurol.* **529**, 828–852 (2021).
16. Amunts, K. *et al.* Cytoarchitectonic mapping of the human amygdala, hippocampal region and entorhinal cortex: intersubject variability and probability maps. *Anat. Embryol. (Berl.)* **210**, 343–352 (2005).
17. Kahn, I., Andrews-Hanna, J. R., Vincent, J. L., Snyder, A. Z. & Buckner, R. L. Distinct cortical anatomy linked to subregions of the medial temporal lobe revealed by intrinsic functional connectivity. *J. Neurophysiol.* **100**, 129–139 (2008).
18. Libby, L. A., Ekstrom, A. D., Ragland, J. D. & Ranganath, C. Differential connectivity of perirhinal and parahippocampal cortices within human hippocampal subregions revealed by high-resolution functional imaging. *J. Neurosci.* **32**, 6550–6560 (2012).
19. Maass, A., Berron, D., Libby, L. A., Ranganath, C. & Düzel, E. Functional subregions of the human entorhinal cortex. *eLife* **4**, e06426 (2015).
20. Plachti, A. *et al.* Multimodal parcellations and extensive behavioral profiling tackling the hippocampus gradient. *Cereb. Cortex* **29**, 1–18 (2019).

21. Grady, C. Meta-analytic and functional connectivity evidence from functional magnetic resonance imaging for an anterior to posterior gradient of function along the hippocampal axis. *Hippocampus* **2019**, 1–16 (2019).
22. Persson, J., Stening, E., Nordin, K. & Söderlund, H. Predicting episodic and spatial memory performance from hippocampal resting-state functional connectivity: Evidence for an anterior–posterior division of function. *Hippocampus* **28**, 53–66 (2018).
23. Poppenk, J., Evensmoen, H. R., Moscovitch, M. & Nadel, L. Long-axis specialization of the human hippocampus. *Trends Cogn. Sci.* **17**, 230–240 (2013).
24. Lladó, A. *et al.* The hippocampal longitudinal axis—relevance for underlying tau and TDP-43 pathology. *Neurobiol. Aging* **70**, 1–9 (2018).
25. Small, S. A., Schobel, S. A., Buxton, R. B., Witter, M. P. & Barnes, C. A. A pathophysiological framework of hippocampal dysfunction in ageing and disease. *Nat. Rev. Neurosci.* **12**, 585–601 (2011).
26. Dalton, M. A., McCormick, C. & Maguire, E. A. Differences in functional connectivity along the anterior-posterior axis of human hippocampal subfields. *NeuroImage* **192**, 38–51 (2019).
27. Ezama, L., Hernández-Cabrera, J. A., Seoane, S., Pereda, E. & Janssen, N. Functional connectivity of the hippocampus and its subfields in resting-state networks. *Eur. J. Neurosci.* **53**, 3378–3393 (2021).
28. Aggleton, J. P. Multiple anatomical systems embedded within the primate medial temporal lobe: Implications for hippocampal function. *Neurosci. Biobehav. Rev.* **36**, 1579–1596 (2012).
29. Strange, B. A., Witter, M. P., Lein, E. S. & Moser, E. I. Functional organization of the hippocampal longitudinal axis. *Nat. Rev. Neurosci.* **15**, 655–669 (2014).
30. Witter, M. P., Hoesen, G. V. & Amaral, D. G. Topographical organization of the entorhinal projection to the dentate gyrus of the monkey. *J. Neurosci.* **9**, 216–228 (1989).
31. Vogel, J. W. *et al.* A molecular gradient along the longitudinal axis of the human hippocampus informs large-scale behavioral systems. *Nat. Commun.* **11**, 960 (2020).
32. Beaujoin, J. *et al.* Post-mortem inference of the human hippocampal connectivity and microstructure using ultra-high field diffusion MRI at 11.7 T. *Brain Struct. Funct.* **223**, 2157–2179 (2018).
33. Dalton, M. A., D'Souza, A., Lv, J. & Calamante, F. New insights into anatomical connectivity along the anterior–posterior axis of the human hippocampus using in vivo quantitative fibre tracking. *eLife* **11**, e76143 (2022).
34. Genon, S., Bernhardt, B. C., La Joie, R., Amunts, K. & Eickhoff, S. B. The many dimensions of human hippocampal organization and (dys)function. *Trends Neurosci.* (2021) doi:10.1016/j.tins.2021.10.003.
35. Buckner, R. L., Andrews-Hanna, J. R. & Schacter, D. L. The brain's default network. *Ann. N. Y. Acad. Sci.* **1124**, 1–38 (2008).
36. Ritchey, M. & Cooper, R. A. Deconstructing the posterior medial episodic network. *Trends Cogn. Sci.* **24**, 451–465 (2020).
37. Schacter, D. L., Addis, D. R. & Buckner, R. L. Remembering the past to imagine the future: the prospective brain. *Nat. Rev. Neurosci.* **8**, 657–661 (2007).
38. Spreng, R. N., Mar, R. A. & Kim, A. S. N. The Common Neural Basis of Autobiographical Memory, Prospection, Navigation, Theory of Mind, and the Default Mode: A Quantitative Meta-analysis. *J. Cogn. Neurosci.* **21**, 489–510 (2008).
39. Adnan, A. *et al.* Distinct hippocampal functional networks revealed by tractography-based parcellation. *Brain Struct. Funct.* **221**, 2999–3012 (2016).

40. Poppenk, J. & Moscovitch, M. A hippocampal marker of recollection memory ability among healthy young adults: contributions of posterior and anterior segments. *Neuron* **72**, 931–937 (2011).
41. Qin, S. *et al.* Large-scale intrinsic functional network organization along the long axis of the human medial temporal lobe. *Brain Struct. Funct.* **221**, 3237–3258 (2016).
42. Insausti, R. & Muñoz, M. Cortical projections of the non-entorhinal hippocampal formation in the cynomolgus monkey (Macaca fascicularis). *Eur. J. Neurosci.* **14**, 435–451 (2001).
43. Blessing, E. M., Beissner, F., Schumann, A., Brünner, F. & Bär, K.-J. A data-driven approach to mapping cortical and subcortical intrinsic functional connectivity along the longitudinal hippocampal axis. *Hum. Brain Mapp.* **37**, 462–476 (2016).
44. Chase, H. W. *et al.* Evidence for an anterior–posterior differentiation in the human hippocampal formation revealed by meta-analytic parcellation of fMRI coordinate maps: Focus on the subiculum. *NeuroImage* **113**, 44–60 (2015).
45. Zhong, Q. *et al.* Functional parcellation of the hippocampus from resting-state dynamic functional connectivity. *Brain Res.* **1715**, 165–175 (2019).
46. Langnes, E. *et al.* Anterior and posterior hippocampus macro- and microstructure across the lifespan in relation to memory—A longitudinal study. *Hippocampus* 1–15 (2020) doi:10.1002/hipo.23189.
47. Huntenburg, J. M., Bazin, P.-L. & Margulies, D. S. Large-Scale Gradients in Human Cortical Organization. *Trends Cogn. Sci.* **22**, 21–31 (2018).
48. Margulies, D. S. *et al.* Situating the default-mode network along a principal gradient of macroscale cortical organization. *Proc. Natl. Acad. Sci.* **113**, 12574–12579 (2016).
49. Shafiei, G. *et al.* Topographic gradients of intrinsic dynamics across neocortex. *eLife* **9**, e62116 (2020).
50. Katsumi, Y. *et al.* Correspondence of functional connectivity gradients across human isocortex, cerebellum, and hippocampus. *Commun. Biol.* **6**, 1–13 (2023).
51. vos de Wael, R. *et al.* Anatomical and microstructural determinants of hippocampal subfield functional connectome embedding. *Proc. Natl. Acad. Sci.* **115**, 10154–10159 (2018).
52. Tian, Y., Margulies, D. S., Breakspear, M. & Zalesky, A. Topographic organization of the human subcortex unveiled with functional connectivity gradients. *Nat. Neurosci.* **23**, 1421–1432 (2020).
53. Przeździk, I., Faber, M., Fernández, G., Beckmann, C. F. & Haak, K. V. The functional organisation of the hippocampus along its long axis is gradual and predicts recollection. *Cortex* **119**, 324–335 (2019).
54. Pang, J. C. *et al.* Geometric constraints on human brain function. *Nature* 1–9 (2023) doi:10.1038/s41586-023-06098-1.
55. Watson, D. M. & Andrews, T. J. Connectopic mapping techniques do not reflect functional gradients in the brain. *NeuroImage* 120228 (2023) doi:10.1016/j.neuroimage.2023.120228.
56. Van Essen, D. C. *et al.* The WU-Minn Human Connectome Project: An overview. *NeuroImage* **80**, 62–79 (2013).
57. Edelmann, E. & Lessmann, V. Dopaminergic innervation and modulation of hippocampal networks. *Cell Tissue Res.* **373**, 711–727 (2018).
58. El-Ghundi, M., O'Dowd, B. F. & George, S. R. Insights into the role of dopamine receptor systems in learning and memory. *Rev. Neurosci.* **18**, 37–66 (2007).
59. Seamans, J. K. & Yang, C. R. The principal features and mechanisms of dopamine modulation in the prefrontal cortex. *Prog. Neurobiol.* **74**, 1–58 (2004).

60. Pedersen, R., Johansson, J. & Salami, A. Dopamine D1-signaling modulates maintenance of functional network segregation in aging. *Aging Brain* **3**, 100079 (2023).
61. Gasbarri, A., Verney, C., Innocenzi, R., Campana, E. & Pacitti, C. Mesolimbic dopaminergic neurons innervating the hippocampal formation in the rat: a combined retrograde tracing and immunohistochemical study. *Brain Res.* **668**, 71–79 (1994).
62. Ishikawa, K., Ott, T. & McGaugh, J. L. Evidence for dopamine as a transmitter in dorsal hippocampus. *Brain Res.* **232**, 222–226 (1982).
63. Kempadoo, K. A., Mosharov, E. V., Choi, S. J., Sulzer, D. & Kandel, E. R. Dopamine release from the locus coeruleus to the dorsal hippocampus promotes spatial learning and memory. *Proc. Natl. Acad. Sci.* **113**, 14835–14840 (2016).
64. Verney, C. *et al.* Morphological evidence for a dopaminergic terminal field in the hippocampal formation of young and adult rat. *Neuroscience* **14**, 1039–1052 (1985).
65. Dubovyk, V. & Manahan-Vaughan, D. Gradient of expression of dopamine D2 receptors along the dorso-ventral axis of the hippocampus. *Front. Synaptic Neurosci.* **11**, (2019).
66. Kahn, I. & Shohamy, D. Intrinsic connectivity between the hippocampus, nucleus accumbens and ventral tegmental area in humans. *Hippocampus* **23**, 187–192 (2013).
67. Nordin, K. *et al.* Distinct and Common Large-Scale Networks of the Hippocampal Long Axis in Older Age: Links to Episodic Memory and Dopamine D2 Receptor Availability. *Cereb. Cortex* **31**, 3435–3450 (2021).
68. Nyberg, L. *et al.* Dopamine D2 receptor availability is linked to hippocampal–caudate functional connectivity and episodic memory. *Proc. Natl. Acad. Sci.* **113**, 7918–7923 (2016).
69. Pedersen, R. *et al.* Dopamine D1-receptor Organization Contributes to Functional Brain Architecture. Preprint at (2023).
70. Froudist-Walsh, S. *et al.* A dopamine gradient controls access to distributed working memory in the large-scale monkey cortex. *Neuron* **109**, 3500-3520.e13 (2021).
71. Nyberg, L., Andersson, M., Lundquist, A., Salami, A. & Wåhlin, A. Frontal contribution to hippocampal hyperactivity during memory encoding in aging. *Front. Mol. Neurosci.* **12**, 1–11 (2019).
72. Salami, A., Pudas, S. & Nyberg, L. Elevated hippocampal resting-state connectivity underlies deficient neurocognitive function in aging. *Proc. Natl. Acad. Sci.* **111**, 17654–17659 (2014).
73. Salami, A., Wåhlin, A., Kaboodvand, N., Lundquist, A. & Nyberg, L. Longitudinal evidence for dissociation of anterior and posterior MTL resting-state connectivity in aging: links to perfusion and memory. *Cereb. Cortex* **26**, 3953–3963 (2016).
74. Berron, D. *et al.* Early stages of tau pathology and its associations with functional connectivity, atrophy and memory. *Brain* **144**, 2771–2783 (2021).
75. de Flores, R. *et al.* Medial Temporal Lobe Networks in Alzheimer's Disease: Structural and Molecular Vulnerabilities. *J. Neurosci.* **42**, 2131–2141 (2022).
76. Harrison, T. M. *et al.* Tau deposition is associated with functional isolation of the hippocampus in aging. *Nat. Commun.* **10**, 1–12 (2019).
77. Haak, K. V., Marquand, A. F. & Beckmann, C. F. Connectopic mapping with resting-state fMRI. *NeuroImage* **170**, 83–94 (2018).
78. Nordin, K. *et al.* DyNAMiC: A prospective longitudinal study of dopamine and brain connectomes: A new window into cognitive aging. *J. Neurosci. Res.* 1–25 (2022) doi:10.1002/jnr.25039.
79. Nilsson, L.-G. *et al.* Betula: A Prospective Cohort Study on Memory, Health and Aging. *Aging Neuropsychol. Cogn.* **11**, 134–148 (2004).

80. Nyberg, L. *et al.* Biological and environmental predictors of heterogeneity in neurocognitive ageing: Evidence from Betula and other longitudinal studies. *Ageing Res. Rev.* **64**, 101184 (2020).
81. Yeo, B. T. *et al.* The organization of the human cerebral cortex estimated by intrinsic functional connectivity. *J. Neurophysiol.* **106**, 1125–1165 (2011).
82. de Flores, R. *et al.* Intrinsic connectivity of hippocampal subfields in normal elderly and mild cognitive impairment patients. *Hum. Brain Mapp.* **38**, 4922–4932 (2017).
83. Paquola, C. *et al.* Convergence of cortical types and functional motifs in the human mesiotemporal lobe. *eLife* **9**, e60673 (2020).
84. Duncan, J. The multiple-demand (MD) system of the primate brain: mental programs for intelligent behaviour. *Trends Cogn. Sci.* **14**, 172–179 (2010).
85. Fedorenko, E., Duncan, J. & Kanwisher, N. Broad domain generality in focal regions of frontal and parietal cortex. *Proc. Natl. Acad. Sci.* **110**, 16616–16621 (2013).
86. Yarkoni, T., Poldrack, R. A., Nichols, T. E., Van Essen, D. C. & Wager, T. D. Large-scale automated synthesis of human functional neuroimaging data. *Nat. Methods* **8**, 665–670 (2011).
87. Dukart, J. *et al.* Cerebral blood flow predicts differential neurotransmitter activity. *Sci. Rep.* **8**, 4074 (2018).
88. Oldehinkel, M. *et al.* Mapping dopaminergic projections in the human brain with resting-state fMRI. *eLife* **11**, e71846 (2022).
89. Thorp, J. N., Gasser, C., Blessing, E. & Davachi, L. Data-Driven Clustering of Functional Signals Reveals Gradients in Processing Both within the Anterior Hippocampus and across Its Long Axis. *J. Neurosci.* **42**, 7431–7441 (2022).
90. Fox, M. D. *et al.* The human brain is intrinsically organized into dynamic, anticorrelated functional networks. *Proc. Natl. Acad. Sci.* **102**, 9673–9678 (2005).
91. Hansen, J. Y. *et al.* Mapping gene transcription and neurocognition across human neocortex. *Nat. Hum. Behav.* **5**, 1240–1250 (2021).
92. Valk, S. L. *et al.* Shaping brain structure: Genetic and phylogenetic axes of macroscale organization of cortical thickness. *Sci. Adv.* **6**, eabb3417 (2020).
93. Goulas, A., Margulies, D. S., Bezgin, G. & Hilgetag, C. C. The architecture of mammalian cortical connectomes in light of the theory of the dual origin of the cerebral cortex. *Cortex* **118**, 244–261 (2019).
94. Pandya, D., Petrides, M. & Cipolloni, P. B. *Cerebral Cortex: Architecture, Connections, and the Dual Origin Concept*. (Oxford University Press, 2015).
95. Lee, A., Yeung, L.-K. & Barense, M. The hippocampus and visual perception. *Front. Hum. Neurosci.* **6**, (2012).
96. Turk-Browne, N. B. The hippocampus as a visual area organized by space and time: A spatiotemporal similarity hypothesis. *Vision Res.* **165**, 123–130 (2019).
97. Huang, C.-C., Rolls, E. T., Hsu, C.-C. H., Feng, J. & Lin, C.-P. Extensive Cortical Connectivity of the Human Hippocampal Memory System: Beyond the “What” and “Where” Dual Stream Model. *Cereb. Cortex* **31**, 4652–4669 (2021).
98. Rolls, E. T., Deco, G., Huang, C.-C. & Feng, J. The effective connectivity of the human hippocampal memory system. *Cereb. Cortex* **32**, 3706–3725 (2022).
99. Stark, S. M., Frithsen, A. & Stark, C. E. L. Age-related alterations in functional connectivity along the longitudinal axis of the hippocampus and its subfields. *Hippocampus* **31**, 11–27 (2021).
100. Hyman, B. T., Van Hoesen, G. W., Damasio, A. R. & Barnes, C. L. Alzheimer’s Disease: Cell-Specific Pathology Isolates the Hippocampal Formation. *Science* **225**, 1168–1170 (1984).

101. Salami, A. *et al.* Association of APOE ε4 and Plasma p-tau181 with Preclinical Alzheimer's Disease and Longitudinal Change in Hippocampus Function. *J. Alzheimers Dis.* **85**, 1309–1320 (2022).
102. Adams, J. N. *et al.* Entorhinal–Hippocampal Circuit Integrity Is Related to Mnemonic Discrimination and Amyloid-β Pathology in Older Adults. *J. Neurosci.* **42**, 8742–8753 (2022).
103. Yassa, M. A., Muftuler, L. T. & Stark, C. E. L. Ultrahigh-resolution microstructural diffusion tensor imaging reveals perforant path degradation in aged humans in vivo. *Proc. Natl. Acad. Sci.* **107**, 12687–12691 (2010).
104. Grady, C., Sarraf, S., Saverino, C. & Campbell, K. Age differences in the functional interactions among the default, frontoparietal control, and dorsal attention networks. *Neurobiol. Aging* **41**, 159–172 (2016).
105. Hughes, C., Faskowitz, J., Cassidy, B. S., Sporns, O. & Krendl, A. C. Aging relates to a disproportionately weaker functional architecture of brain networks during rest and task states. *NeuroImage* **209**, 116521 (2020).
106. Pedersen, R. *et al.* When functional blurring becomes deleterious: Reduced system segregation is associated with less white matter integrity and cognitive decline in aging. *NeuroImage* **242**, 118449 (2021).
107. Spreng, R. N., Stevens, W. D., Viviano, J. D. & Schacter, D. L. Attenuated anticorrelation between the default and dorsal attention networks with aging: evidence from task and rest. *Neurobiol. Aging* **45**, 149–160 (2016).
108. Whitfield-Gabrieli, S. & Ford, J. M. Default Mode Network Activity and Connectivity in Psychopathology. *Annu. Rev. Clin. Psychol.* **8**, 49–76 (2012).
109. Zhang, J. *et al.* What have we really learned from functional connectivity in clinical populations? *NeuroImage* **242**, 118466 (2021).
110. Mulders, P. C., van Eijndhoven, P. F., Schene, A. H., Beckmann, C. F. & Tendolkar, I. Resting-state functional connectivity in major depressive disorder: A review. *Neurosci. Biobehav. Rev.* **56**, 330–344 (2015).
111. Wang, Y. *et al.* Disrupted effective connectivity of the default, salience and dorsal attention networks in major depressive disorder: a study using spectral dynamic causal modelling of resting-state fMRI. *J. Psychiatry Neurosci.* **47**, E421–E434 (2022).
112. Whitfield-Gabrieli, S. *et al.* Hyperactivity and hyperconnectivity of the default network in schizophrenia and in first-degree relatives of persons with schizophrenia. *Proc. Natl. Acad. Sci.* **106**, 1279–1284 (2009).
113. Weiler, M. *et al.* Intranetwork and internetwork connectivity in patients with Alzheimer disease and the association with cerebrospinal fluid biomarker levels. *J. Psychiatry Neurosci.* **42**, 366–377 (2017).
114. Zuo, N., Salami, A., Liu, H., Yang, Z. & Jiang, T. Functional maintenance in the multiple demand network characterizes superior fluid intelligence in aging. *Neurobiol. Aging* **85**, 145–153 (2020).
115. Cabeza, R. *et al.* Maintenance, reserve and compensation: the cognitive neuroscience of healthy ageing. *Nat. Rev. Neurosci.* **19**, 701 (2018).
116. Nyberg, L., Lövdén, M., Riklund, K., Lindenberger, U. & Bäckman, L. Memory aging and brain maintenance. *Trends Cogn. Sci.* **16**, 292–305 (2012).
117. Haak, K. V. & Beckmann, C. F. Understanding brain organisation in the face of functional heterogeneity and functional multiplicity. *NeuroImage* **220**, 117061 (2020).
118. Nevalainen, N. *et al.* COBRA: A prospective multimodal imaging study of dopamine, brain structure and function, and cognition. *Brain Res.* **1612**, 83–103 (2015).
119. Fischl, B. *et al.* Whole brain segmentation: Automated labeling of neuroanatomical structures in the human brain. *Neuron* **33**, 341–355 (2002).

120. Fischl, B. *et al.* Sequence-independent segmentation of magnetic resonance images. *NeuroImage* **23, Supplement 1**, S69–S84 (2004).
121. Buckner, R. L. *et al.* A unified approach for morphometric and functional data analysis in young, old, and demented adults using automated atlas-based head size normalization: reliability and validation against manual measurement of total intracranial volume. *NeuroImage* **23**, 724–738 (2004).
122. Jack, C. R. *et al.* Anterior temporal lobes and hippocampal formations: normative volumetric measurements from MR images in young adults. *Radiology* **172**, 549–554 (1989).
123. Ciric, R. *et al.* Benchmarking of participant-level confound regression strategies for the control of motion artifact in studies of functional connectivity. *NeuroImage* **154**, 174–187 (2017).
124. Satterthwaite, T. D. *et al.* An improved framework for confound regression and filtering for control of motion artifact in the preprocessing of resting-state functional connectivity data. *NeuroImage* **64**, 240–256 (2013).
125. Hallquist, M. N., Hwang, K. & Luna, B. The nuisance of nuisance regression: Spectral misspecification in a common approach to resting-state fMRI preprocessing reintroduces noise and obscures functional connectivity. *NeuroImage* **82**, 208–225 (2013).
126. Ashburner, J. A fast diffeomorphic image registration algorithm. *NeuroImage* **38**, 95–113 (2007).
127. Innis, R. B. *et al.* Consensus Nomenclature for in vivo Imaging of Reversibly Binding Radioligands: *J. Cereb. Blood Flow Metab.* **27**, 1533–1539 (2007).
128. Lammertsma, A. A. & Hume, S. P. Simplified Reference Tissue Model for PET Receptor Studies. *NeuroImage* **4**, 153–158 (1996).
129. Greve, D. N. *et al.* Different partial volume correction methods lead to different conclusions: An 18F-FDG-PET study of aging. *NeuroImage* **132**, 334–343 (2016).
130. Jenkinson, M., Beckmann, C. F., Behrens, T. E. J., Woolrich, M. W. & Smith, S. M. FSL. *NeuroImage* **62**, 782–790 (2012).
131. Smith, S. M. *et al.* Advances in functional and structural MR image analysis and implementation as FSL. *NeuroImage* **23**, S208–S219 (2004).
132. Marcus, D. S. *et al.* Human Connectome Project informatics: Quality control, database services, and data visualization. *NeuroImage* **80**, 202–219 (2013).
133. Schaefer, A. *et al.* Local-Global Parcellation of the Human Cerebral Cortex from Intrinsic Functional Connectivity MRI. *Cereb. Cortex* **28**, 3095–3114 (2018).
134. Alexander-Bloch, A. F. *et al.* On testing for spatial correspondence between maps of human brain structure and function. *NeuroImage* **178**, 540–551 (2018).